THE JOURNAL OF BIOLOGICAL CHEMISTRY VOL. 290, NO. 4, pp. 2086–2098, January 23, 2015

Molecular Determinants of Phosphatidylinositol 4,5-Bisphosphate ($PI(4,5)P_2$) Binding to Transient Receptor Potential V1 (TRPV1) Channels*

Received for publication, October 8, 2014, and in revised form, November 18, 2014 Published, JBC Papers in Press, November 25, 2014, DOI 10.1074/jbc.M114.613620

Horacio Poblete[‡1], Ingrid Oyarzún[§1], Pablo Olivero[¶], Jeffrey Comer[‖], Matías Zuñiga[**], Romina V. Sepulveda[‡‡§§], David Báez-Nieto[§], Carlos González Leon[§], Fernando González-Nilo[§ §§2], and Ramón Latorre[§3]

From the [‡]Center for Bioinformatics and Molecular Simulation, Universidad de Talca, 2 Norte 685, Talca-Chile, [§]Centro Interdisciplinario de Neurociencia de Valparaíso, Facultad de Ciencias, Universidad de Valparaíso, Valparaíso 2366103, Chile, [¶]Escuela de Medicina, Universidad de Valparaíso, Hontaneda 2664, Valparaíso, Chile, [‖]Institute of Computational Comparative Medicine, Department of Anatomy and Physiology, Kansas State University, P-200 Mosier Hall, Manhattan, Kansas 66506-5802, [**]Doctorado Fisicoquímica Molecular, Universidad Andrés Bello, Ave, Republica 275, Santiago, Chile, [‡‡]Doctorado en Biotecnología, Universidad Andrés Bello, Av. Republica 217, Santiago, Chile, and [§§]Center for Bioinformatics and Integrative Biology, Facultad de Ciencias Biológicas, Universidad Andrés Bello, Av. República 239, Santiago, Chile

Background: The mode of action of $PI(4,5)P_2$ in TRPV1 is controversial.
Results: Positively charged amino acids in the S4-S5 linker and in the TRP box form the $PI(4,5)P_2$ binding site.
Conclusion: $PI(4,5)P_2$ is a TRPV1 agonist and induces a conformational change of the internal gate.
Significance: The molecular nature of the $PI(4,5)P_2$ binding site in TRPV1 is defined.

Phosphatidylinositol 4,5-bisphosphate ($PI(4,5)P_2$) has been recognized as an important activator of certain transient receptor potential (TRP) channels. More specifically, TRPV1 is a pain receptor activated by a wide range of stimuli. However, whether or not $PI(4,5)P_2$ is a TRPV1 agonist remains open to debate. Utilizing a combined approach of mutagenesis and molecular modeling, we identified a $PI(4,5)P_2$ binding site located between the TRP box and the S4-S5 linker. At this site, $PI(4,5)P_2$ interacts with the amino acid residues Arg-575 and Arg-579 in the S4-S5 linker and with Lys-694 in the TRP box. We confirmed that $PI(4,5)P_2$ behaves as a channel agonist and found that Arg-575, Arg-579, and Lys-694 mutations to alanine reduce $PI(4,5)P_2$ binding affinity. Additionally, *in silico* mutations R575A, R579A, and K694A showed that the reduction in binding affinity results from the delocalization of $PI(4,5)P_2$ in the binding pocket. Molecular dynamics simulations indicate that $PI(4,5)P_2$ binding induces conformational rearrangements of the structure formed by S6 and the TRP domain, which cause an opening of the lower TRPV1 channel gate.

Of the thermo-TRP channels known to date, the transient receptor potential vanilloid 1 (TRPV1),[4] which was the first to be cloned, is activated by temperature increases in the noxious range and by capsaicin (CAP), which is the pungent ingredient of chili peppers (1, 2). TRPV1 channels, which are found in a subset of neurons in the dorsal root and trigeminal ganglia, have been implicated in thermal nociception, specifically in inflammation-induced thermal hyperalgesia (3–5). TRPV1 is a nonselective cation channel that works as a polymodal signal integrator of chemical and physical stimuli, such as activation by CAP, anandamide, heat, and protons. At the structural level, TRPV1 is a homotetramer, where each subunit has six transmembrane segments (*i.e.* S1-S6) with the N and C termini located in the intracellular region (6, 7). Recently, a three-dimensional structure of the TRPV1 channel has been determined at a resolution of 3.3 Å by cryo-electron microscopy. Moreover, the structure of TRPV1 in complex with two potent agonists, namely resiniferatoxin (RTX; Ref. 1) and the spider double-knot toxin (Ref. 8; DkTx), as well as TRPV1 in complex with CAP were determined at resolutions of 3.8 and 4.2 Å, respectively (9, 10).

With regard to phosphatidylinositol 4,5-bisphosphate ($PI(4,5)P_2$), while it is agreed that the C terminus contains a $PI(4,5)P_2$ binding site (9, 11–13), there is still debate as to whether $PI(4,5)P_2$ behaves as an activator (13, 14) or as a TRPV1 channel antagonist, as recently proposed by (15). Regardless of whether $PI(4,5)P_2$ activates TRPV1 or exerts an inhibitory effect, it may be safe to assume that the negatively charged headgroups of $PI(4,5)P_2$ should be in contact with positively charged regions of the TRPV1 channel. A molecular simulation showed that a $PI(4,5)P_2$ headgroup made contact with positively charged res-

* This work was supported by the Centro Interdisciplinario de Neurociencia de Valparaíso (CINV), a Millennium Institute supported by the Millennium Scientific Initiative of the Ministerio de Economía, Fomento y Turismo. This work was also supported by the Doctoral Program of Applied Sciences at Talca University, as well as CONICYT-Chile for a doctoral fellowship and Project FONDECYT 3140288 (to H. P.), the Project FONDECYT 1110430 (to R. L.) and 1131003 (to F. G. N.), and Anillo Cientifico ACT-1107 (to F. G. N.) and Anillo ACT-1104 (to C. G. L.), Grant RI-130006 (to R. L. and C. G.) and Project FONDECYT 11100047 (to P. O.).
[1] These authors contributed equally to this work.
[2] To whom correspondence may be addressed: Universidad Andrés Bello, Center for Bioinformatics and Integrative Biology, Facultad de Ciencias Biológicas, Av. República 239, Santiago, Chile. E-mail: fernando.gonzalez@unab.cl.
[3] To whom correspondence may be addressed: Centro Interdisciplinario de Neurociencia de Valparaíso, Facultad de Ciencias, Universidad de Valparaíso, Valparaíso 2366103, Chile. E-mail: ramon.latorre@uv.cl.

[4] The abbreviations used are: TRPV, transient receptor potential vanilloid; $PI(4,5)P_2$, phosphatidylinositol 4,5-bisphosphate; CAP, capsaicin; MD, molecular dynamics; PME, particle-mesh Ewald.

idues Lys-694, Lys-698, and Lys-701 from the proximal TRPV1 C terminus, and with amino acids Arg-575 and Arg-579 located in the S4-S5 linker (11). This finding is consistent with the notion that the negatively charged PI(4,5)P_2 headgroup should bind to a positively charged TRPV1 region in the vicinity of the bilayer surface. In fact, a deletion analysis of the distal C-terminal region of TRPV1 showed that this segment is not required for TRPV1 to be regulated by PI(4,5)P_2, while, in contrast, the proximal C-terminal fragment was observed to interact directly with PI(4,5)P_2 *in vitro* (13).

In the present study, by using electrophysiology, mutagenesis and by performing atomistic molecular dynamics (MD) and docking simulations, we observed that PI(4,5)P_2 behaves as a channel agonist and we were able to unveil the binding site for PI(4,5)P_2 in the TRPV1 channel. The molecular simulations also allowed us to identify the structural rearrangements that the channel undergoes upon PI(4,5)P_2 binding.

EXPERIMENTAL PROCEDURES

Molecular Biology—cDNA coding for rat TRPV1 (GenBank™ accession no. NM031982) cloned in pcDNA3 vector was used. All mutants were generated by Quickchange mutagenesis (Stratagene, La Jolla, CA), according to the manufacturer's instructions, using the sense and antisense primers. All clones were confirmed by DNA sequencing.

Cell Culture and Transfection—HeLa and HEK 293 cells were transfected with pcDNA3 vector containing the wild-type or mutant coding sequence, so as to show that the effects are independent of the cell expression system. Transfection was carried out by using the FuGENE® 6 Transfection Reagent (Promega).

PI(4,5)P_2—All phosphoinositides were the short-chain DiC8 versions. DiC8-PI(4,5)P_2 solutions were solubilized in recording solution from 1 mM stock, frozen at −20 °C, and used the same day they were diluted from the stock.

Electrophysiology—For electrophysiological experiments, culture cells were grown on 12-mm cover slips and were directly mounted in the experimental chamber installed on the stage of an inverted microscope (Olympus). Inside-out excised patch recordings were performed at 20 °C using filamented borosilicate glass pipettes (o.d. = 1.5 mm, i.d. = 0.86 mm, Warner Instruments, Hamden, CT) that had been heat-polished with a microforge. Patch pipettes (tip size, 3–4 μm) were filled with saline solution (150 mM NaCl, 10 mM EGTA, 2 mM $MgCl_2$, 10 mM HEPES, pH 7.4), and the same solution was also used as the external recording solution. All experiments were performed at 20 °C using the following voltage protocol: hp = 0 mV, and the membrane was pulsed to voltages between −100 and +220 mV in 20 mV increments for 30 ms, each followed by a step to −80 mV. Currents were recorded with an *Axopatch 200B* system (Axon Instruments), filtered at 1 kHz using a low-pass 10-pole Bessel filter, and transferred to a computer using a *Digidata interface* (Axon Instruments) at a sampling rate of 20 kHz. CAP was dissolved in ethanol to a final concentration of 1 mM in ethanol and then diluted to the desired concentrations on the day of the experiment.

Dose-response Curves—All electrophysiological experiments were repeated at least four times. Representative traces are shown in Fig. 1, *A* and *B*. Electrophysiological data were analyzed with Origin Pro (OriginLab Corp. Northampton). All of the results are presented as mean ± S.D. for each experimental condition. CAP responses were obtained at the beginning or end of the recordings for the purpose of TRPV1 expression control. PI(4,5)P_2 enhanced the TRPV1-induced current channel activity when added to inside-out patches already treated with 1 μM CAP. However, PI(4,5)P_2 concentrations over 15 μM was observed to activate endogenous current in HeLa cells, possibly due to the activation of TRPM4 (16). To compare the effect of PI(4,5)P_2 before and after stimulation with CAP, we normalized our recordings to the maximum current obtained with CAP in the presence of 15 μM PI(4,5)P_2 at steady state (Equation 1).

$$I_{Max} = I_{CAP+PIP_2} \quad \text{(Eq. 1)}$$

The experimental data of each patch were fitted (Fig. 1*E*, *solid lines*) as free parameters by using the following Hill Equation 2,

$$\frac{I_{PIP_2}}{I_{Max}} = \frac{[PIP_2]^n}{EC_{50}^n + [PIP_2]^n} \quad \text{(Eq. 2)}$$

where n is the Hill coefficient and EC_{50} is the PI(4,5)P_2 concentration producing 50% of the maximal effect. Statistical significance was assayed with the two-tailed Student's t test or a one-way ANOVA, as appropriate, with Statgraphics Plus 5.0 (GraphPad Software, Inc., San Diego, CA). Statistical significance was considered at $p < 0.05$.

Computational Methods—In this study, we employed a computational method to evaluate the interaction between PI(4,5)P_2 molecules and the wild-type and mutated TRPV1 channels. First, molecular docking simulations of PI(4,5)P_2 for the wild-type channel and for the R575A, R579A, K694A, and R701A mutants were performed. Then, by using the structure obtained from docking simulations as a starting point, the structural and energetic properties of the TRPV1-PI(4,5)P_2, TRPV1-CAP, and TRPV1- PI(4,5)P_2-CAP- complexes were analyzed through molecular dynamics simulations.

Atomistic Protein Systems Preparation—Cryo-electron microscopy structures of the wild-type closed (3J5P) (10) and open (3J5Q) (9) TRPV1 channels were obtained directly from the Protein Data Bank entry. Beginning from the atomic positions in the closed structure, point mutations were made in all four subunits of the TRPV1 channel. Molecular models of the R575A, R579A, R701A, and K694A mutants were thus created by using the plugin *mutator1.3* implemented in the software VMD (17).

Molecular Docking of PI(4,5)P_2 into the TRPV1 Channel—For the purpose of evaluating the most probable PI(4,5)P_2 binding site in the wild-type TRPV1 structure (PDB id:3J5P) (10), we performed docking simulations with the program Molsoft ICM (Internal Coordinate Mechanics) software (18). ICM was used to draw the PI(4,5)P_2 structure, assign bond orders, place explicit hydrogen atoms, identify hydrogen bonds using water sampling and minimize energy using the MMFF94 force field (19). We used a cubic box of 30 × 30 × 45 $Å^3$. Default docking parameters were used. As docking progressed, we utilized a systematic search of PI(4,5)P_2 conformations, followed by the insertion of PI(4,5)P_2 into the wild-type or mutant TRPV1

structures. Subsequently, a minimization of the interaction energy between PI(4,5)P_2 and TRPV1 was performed, as defined by the MMFF94 force field. Finally, the lowest energy configurations were subjected to a Biased Probability Monte Carlo procedure, so as to refine the TRPV1 structure and further reduce the conformational energy (18). This methodology and the same simulation conditions were used to dock PI(4,5)P_2 and CAP into the APO- and CAP-TRPV1 structures (PDB ID:3J5P and 3J5R, respectively) (9, 10).

Molecular Dynamics Simulations of TRPV1 Systems—Beginning from the structures determined by cryo-electron microscopy, we built several TRPV1-membrane systems in atomistic detail. First, we performed 300 ns of simulation to verify that the APO-TRPV1 structure obtained from cryo-electron microscopy remained stable in simulation while embedded in a POPC lipid bilayer membrane. To determine whether we could observe the conformational changes of TRPV1 associated with PI(4,5)P_2 binding, we modified the above system by adding PI(4,5)P_2 (APO-TRPV1- PI(4,5)P_2) in the most favorable configuration determined by docking. Thereafter, the system was unrestrained to reach a total simulation time of 300 ns. Finally, we added 4 CAP molecules (APO-TRPV1- PI(4,5)P_2-CAP) to the APO-TRPV1- PI(4,5)P_2 system, which subsequently was left unrestrained during 200 ns simulation. In addition, an independent system was constructed by inserting PI(4,5)P_2 and CAP into the RTX/DkTx-TRPV1 structure determined experimentally.

The detailed protocols of the molecular dynamics simulations were as follows. All MD simulations were performed with the program NAMD 2.9 (20) and the CHARMM36 force field (21) and analyzed with the software VMD (17). A steady temperature was enforced with a Langevin thermostat, having a damping coefficient of 1 ps^{-1}. A steady pressure of 1 atm was enforced using the Langevin piston method (22). Short-range electrostatic and van der Waals interactions were truncated smoothly from 10 to 12 Å, while long-range electrostatic forces were computed using the particle-mesh Ewald (PME) summation method (23). The parameters and charges for PI(4,5)P_2 and CAP were determined from the ParamChem online server using the CGenFF force field (24). The POPC lipids were modeled using a united-atom modification of the CHARMM36 force field for lipids (25, 26). The POPC bilayer membrane had a lateral area of 160×160 $Å^2$ and was solvated in a periodic box of pre-equilibrated TIP3P water molecules (27) using VMD (17). Potassium and chloride ions (0.11 M KCl) were added to the aqueous phase to mimic the experimental conditions and to guarantee electrical neutrality. The initial configurations of each system were optimized by means of an energy minimization algorithm. Soft harmonic restraints were applied to the protein backbone (0.5 kcal/(mol $Å^2$)) in the first 70 ns of equilibration. Thereafter, the system was unrestrained to reach a total time of 300 ns. When CAP was added, harmonic restraints (2 kcal/(mol $Å^2$)) were assigned to preserve the distance between CAP molecules and residues of the CAP binding site in the first 30 ns of the simulation. The system was then left unrestrained during a 200 ns trajectory. To understand the expansion of the lower gate, two distance restraints (10 kcal/(mol$Å^2$)) were applied between the Cα carbon of the Ile-679 faced. The distance was applied to obtain a radius of 2.2 Å, which is observed into the lower gate in the RTX/DkTx TRPV1: PI(4,5)P_2:CAP simulation. The last stage lasted for 30 ns trajectory.

RESULTS

PI(4,5)P_2 Directly Activates TRPV1 Channels—To study whether PI(4,5)P_2 activates TRPV1 and how this lipid modulates CAP-induced current, the current-voltage relationship was first determined by using inside-out membrane patches expressing TRPV1 channels. In the absence of CAP, no macroscopic current was detected in the voltage range tested. We found that adding PI(4,5)P_2 to the internal solution activated outward current only in cells expressing TRPV1 channels (Fig. 1, *A* and *B*). Moreover, PI(4,5)P_2 alone was observed to activate TRPV1 steady state current in the absence of all stimuli, such as CAP or temperature (Fig. 1, *A* and *C*). As was also reported by Ufret-Vincenty *et al.* (13), we found that PI(4,5)P_2 further enhances TRPV1-induced currents when added to inside-out patches previously treated with 1 μM CAP (Fig. 1, *B* and *D*). PI(4,5)P_2 activation data were fitted with a Hill equation (see under "Experimental Procedures"). Dose-response data were well fitted using an EC_{50} value of 3.2 μM and 5.6 μM as well as Hill coefficients of 1.7 and 1.5 for data obtained in the presence and absence of CAP, respectively (*solid lines* in Fig. 1*E*). PI(4,5)P_2 dose-response data in the presence of CAP is in reasonable agreement with that obtained by Ufret-Vincenty *et al.* (13), and the rightward shift seen in the absence of CAP can be explained on the basis of a simple allosteric model (28, 29) (Fig. 1, *F* and *G*). The main assumption of this model, which is that CAP and PI(4,5)P_2 sensors are contained in separate structures, is corroborated by the structural data (See below, Fig. 4*E*). In this model, PI(4,5)P_2 binding, as described by the equilibrium constant *Q*, facilitated the opening transition through the allosteric factor *F* (LF, $F \gg 1$). CAP addition was observed to further facilitate the opening, since the opening reaction was then determined by LFC ($C \gg 1$), thus promoting a shift to the left of the PI(4,5)P_2 dose-response curve (Fig. 1*E*). It is interesting to note that we consistently found that maximal currents were larger when CAP was added prior to the addition of PI(4,5)P_2 (cf. Fig. 1, *C* and *D*). A possible explanation for this result is provided in the discussion section on the basis of our molecular simulations.

Computational Determination of the Binding Site—To explain the molecular characteristics of PI(4,5)P_2 binding to the TRPV1 channel at the atomic level, molecular docking simulations of PI(4,5)P_2 were performed on the atomistic structure of wild-type TRPV1 (9). The locations of four binding sites for PI(4,5)P_2 in TRPV1 are shown in Fig. 2, *A* and *B*. Fig. 2*D* shows in detail the lowest energy conformation of the 50 docking simulations produced by the software ICM. In most (82%) of these configurations, strong interactions were present between the phosphate at position 5 of the PI(4,5)P_2 headgroup (Fig. 2*C*) and the guanidine groups of residues Arg-575 and Arg-579. The distances between the phosphorus atom and the center of mass of the amino acid were 4 Å and 3 Å, respectively. Additionally, among the conformations produced by docking, the Lys-694 residue was seen to alternate between making contact with the

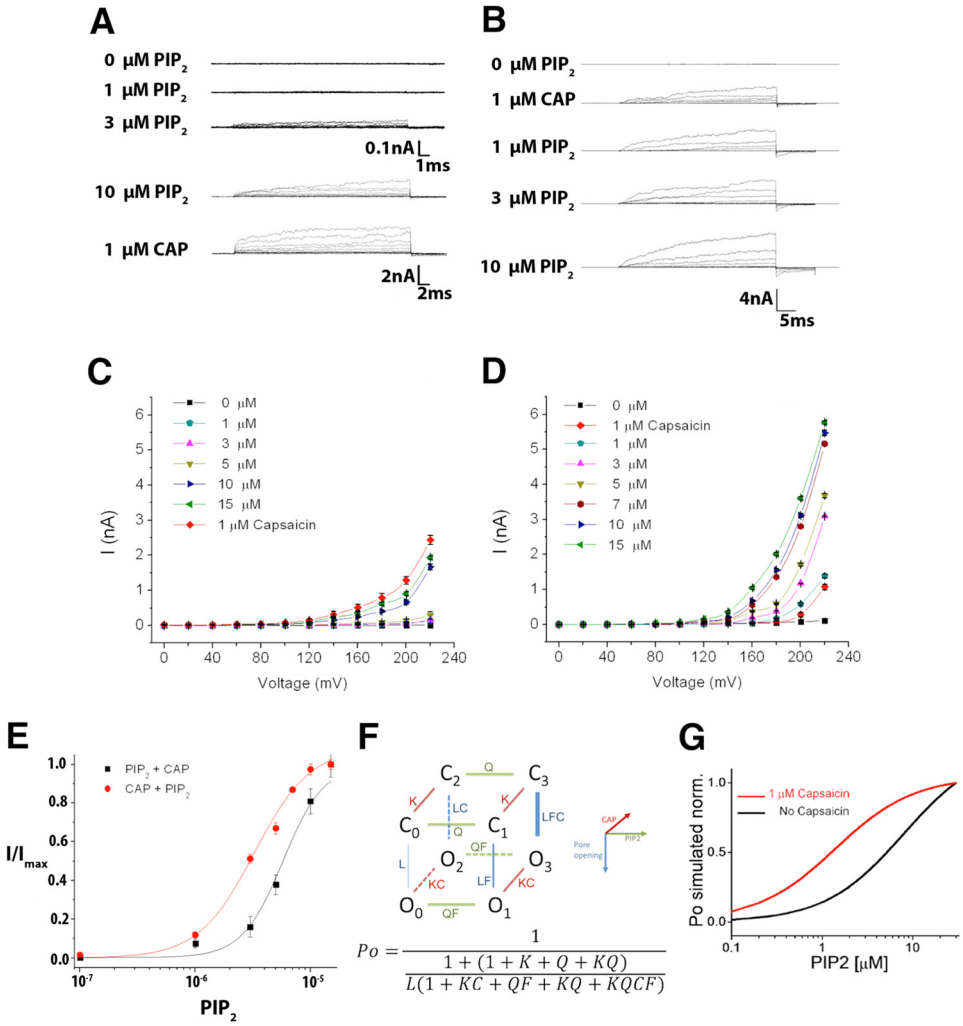

FIGURE 1. **PI(4,5)P_2 directly activates TRPV1 and enhances capsaicin-induced current.** Macroscopic currents for TRPV1 induced by PI(4,5)P_2 before (*A*) and after (*B*) the addition of 1 μM CAP obtained using inside-out patches. Current recordings were obtained in response to voltage pulses from 0 mV to 220 mV in 10 mV steps. This voltage protocol was applied for each concentration of PI(4,5)P_2 before and after 1 μM of CAP in the same patch (n>4). No currents were detected in these voltage ranges in the absence of agonists. Temperature: 20 °C. *C*, current-voltage relationship obtained by adding the indicated PI(4,5)P_2 concentration and adding capsaicin. Each point is the average of measurements on 4 patches. *D*, current-voltage relationship obtained by adding CAP prior to the PI(4,5)P_2 addition. *E*, dose-response curves for TRPV1wild-type treated with PI(4,5)P_2 before and after adding 1 μM CAP. EC_{50} values were 3.2 ± 0.2 μM and 5.6 ± 0.9 μM for respectively (nH = 1.7 and 1.5, n >4). *F*, allosteric model proposed for the activation of the TRPV1 channel by CAP and PI(4,5)P_2. *F*, allosteric model for TRPV1 gating. The opening reaction is described by the equilibrium constant *L* and the binding of PI(4,5)P_2, and CAP by the equilibrium constants *Q* and *K*, respectively. Allosteric factors *F* and *C* facilitate opening when PI(4,5)P_2 and CAP, respectively bind to the channel. *G*, PI(4,5)P_2 dose-response curves. The curves were identified by using the equation given in the figure with $Q = 7$ μM (Fig. 1*E*) and $K = 0.6$ μM (REF. 4) and $C = 1{,}000$ and $D = 10{,}000$.

phosphate located at positions four and five of PI(4,5)P_2. These contacts appeared in ~50% of the conformations. Furthermore, a hydrogen bond was formed between the ester group of one of the hydrocarbon chains of PI(4,5)P_2 and the guanidine group of residue Arg-579 (~2.9 Å) in most (76%) of the generated configurations (Fig. 2*D*). On the other hand, it was unlikely for the Arg-701 residue to form part of the binding pocket of PI(4,5)P_2 because it was far (>12 Å) from PI(4,5)P_2 in 100% of the conformations obtained by docking. In addition to the residues mutated in this work, Lys-571, Lys-688, and Gln-561 appeared to contribute to the binding of PI(4,5)P_2. Moreover, it was possible to identify that the 50 lowest energy docking conformations of PI(4,5)P_2 in the wild-type TRPV1 channel are quite similar, implying a single distinct bound state.

Cationic Residues Identified in Silico Are Involved in PI(4,5)P_2 Activation of TRPV1 in Vivo—Toward the aim of testing the predictions forecasted by our structural models, the residues we identified *in silico* (Arg-575, Arg-579, Lys-694) were experimentally mutated to alanine. We also mutated residue Arg-701 to alanine as a negative control. All the neutralization mutants of TRPV1 were almost identically sensitive to CAP, just like wild-type TRPV1 (data not shown). However, neutralization of residues Arg-575, Arg-579, and Lys-694 (but not Lys-701) strongly affected PI(4,5)P_2-induced activation (Fig. 3*A*) by shifting dose-response curves to the right along the concentration axis (Fig. 3*B*). Thus, mutations of positively charged residues at the proposed PI(4,5)P_2 binding site decreased the apparent affinity of PI(4,5)P_2 to this binding site (Fig. 3*B*). Our results showed that the proximal regions of the S4-S5 linker and the TRP domain show a high affinity for PI(4,5)P_2 and induce TRPV1 activation in the absence of other agonists and at a temperature well below the threshold for this channel.

To identify possible mutation effects on the molecular interactions between PI(4,5)P_2 and its binding site, molecular dock-

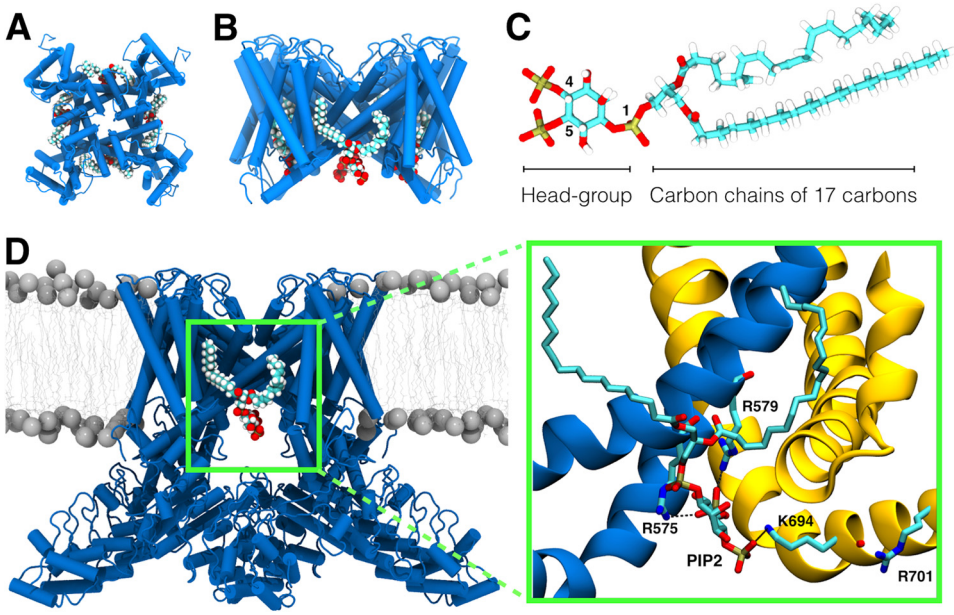

FIGURE 2. **Theoretical search for a putative PI(4,5)P_2 binding site in the TRPV1 channel.** *A* and *B*, top view and side view (with respect to the plane of the membrane) of the TRPV1 channel bound to four PI(4,5)P_2 molecules. *C*, atomistic representation of the PI(4,5)P_2 model. Numbers 1, 4, and 5 indicate the position of the phosphate groups. *D*, conformation of PI(4,5)P_2 in the binding pocket of the wild-type TRPV1 channel. Inset (*dotted green lines*), magnified view of the atomic-level interactions between wild-type TRPV1 and PI(4,5)P_2. Portions of two different subunits are shown. Amino acid residues Arg-575 and Arg-579 are located in the S4-S5 linker of the *blue subunit* and residue Lys-694 is in the TRP domain of the *yellow subunit*.

ing simulations were performed on the structures of the TRPV1 mutants that were obtained *in silico* (R575A, R579A, K694A, and K701A). Fig. 3, *C–L* shows the lowest energy configurations produced by docking PI(4,5)P_2 into the binding pocket of the wild-type and mutant proteins. By observing the data presented in Fig. 3, *D* and *I* (mutant R575A), we arrived at the general conclusion that PI(4,5)P_2 shows a high convergence of configurations when bound to the binding pocket in wild-type TRPV1 (Fig. 3, *C* and *H*). On the other hand, PI(4,5)P_2 was able to bind in a broad range of configurations in the alanine mutants. More specifically, R579A (Fig. 3, *E* and *J*), and K694A (Fig. 3, *F* and *K*) mutants showed a drastic difference in binding mode as compared with the wild-type system. Therefore, the positively charged amino acid residues described above were shown to be key residues for PI(4,5)P_2 binding based on the mutant docking simulations of the mutant TRPV1 channels. In the negative control experiment, PI(4,5)P_2-induced activation of TRPV1 channels was unaltered when a residue outside of the binding pocket (*i.e.* Arg-701) was changed to alanine. Correspondingly, the modeling showed little change in the bound configuration of PI(4,5)P_2 for the R701A mutant (Fig. 3, *G* and *L*). In quantitative terms, the minimum binding energy score predicted by the docking software (ICM) was substantially lower for the wild-type than for any of the mutants, with the exception of the R701A mutant, which exhibited a very similar score to that of the wild-type system.

In summary, the fifty lowest energy configurations produced by docking for each TRPV1 system (Fig. 3, *I–L*) reveal a single strong binding mode for the wild-type and negative control mutant, but many distinct, weakly bound conformations for the other mutants. The single strong binding mode seen in the simulations is associated with PI(4,5)P_2-induced activation of TRPV1 at low PI(4,5)P_2 concentrations in electrophysiological experiments, while the weak binding corresponded to measured PI(4,5)P_2-induced TRPV1 activation only at very high PI(4,5)P_2 concentrations.

TRPV1-PI(4,5)P_2 Complex Stability—To assess the stability of the configuration established by docking and further probe the interactions between PI(4,5)P_2 and the protein, a 300 ns MD simulation was performed and started from the configuration shown in Fig. 2*D*. Fig. 4*A* shows the RMSD of the atomic positions as a function of time with respect to the starting configuration for each PI(4,5)P_2 molecule at the four independent binding sites. These RMSDs generally showed that the molecular conformation slightly diverged in the first few nanoseconds for each PI(4,5)P_2 molecule. This result was expected, due to the approximate nature of the binding energy estimated by the docking software and the fact that the protein was fixed during docking. After about 50 ns, the RMSD saturated at a relatively small value, while maintaining the qualitative features of the optimal configuration as per the docking algorithm. Fig. 4*B* shows that the distances to the Arg-575, Arg-579, and Lys-694 residues remained stable after 50 ns of MD simulation, suggesting that the TRPV1-PI(4,5)P_2 complex was in conformational equilibrium. In particular, the phosphate group at position four of the PI(4,5)P_2 polar headgroup formed a salt bridge with the Arg-575 (~4.2 Å) and Arg-579 (~4.6 Å) NH_3^+ groups (Fig. 2*C*). Additionally, the phosphate group at position five of the PI(4,5)P_2 polar headgroup established another salt bridge with residue Lys-694 (~3.8 Å). Therefore, the key interactions predicted by docking for residues Arg-575, Arg-579, and Lys-694 were maintained, and the side chains of these residues adapted their orientations, which were fixed during docking, to actually increase the strength of the electrostatic interactions.

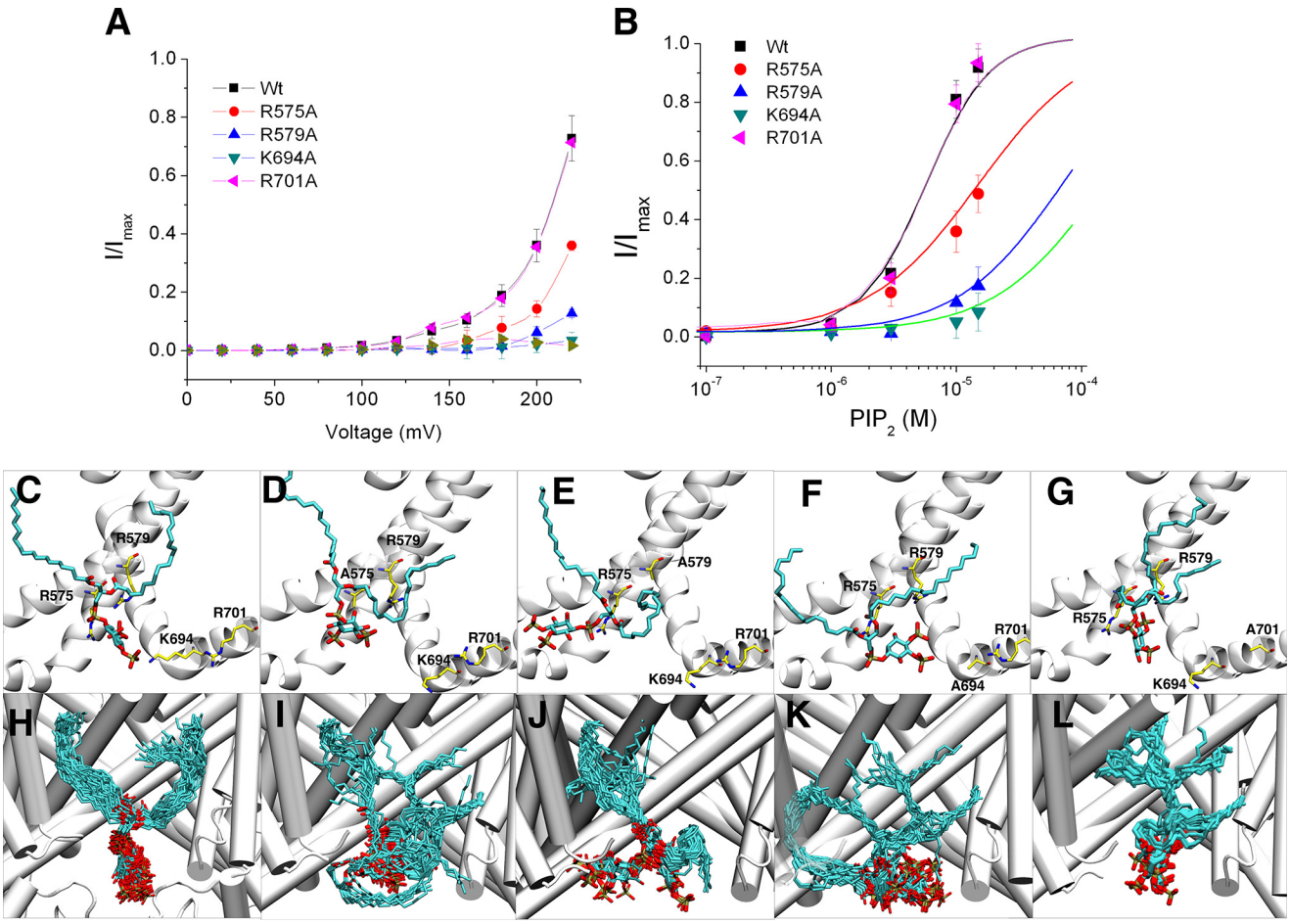

FIGURE 3. **Effects of mutations on the key residues that link PI(4,5)P$_2$ to the TRPV1 channel.** *A*, current-voltage relationships for the wild type TRPV1 and TRPV1 alanine mutants obtained in the presence of 10 μM PI(4,5)P$_2$. *B*, Hill plots for wild-type TRPV1 and alanine mutants. EC_{50} and Hill coefficients were: wild-type: 5.6 μM and 1.5; R575A: 18.5 μM and 1.0; R579A: 73.6 and 1.0; K694A: 88.1 and 1.0; R701A: 5.5 and 1.4. *C–G*, an enlarged view of the lowest energy configurations attained by PI(4,5)P$_2$ in the binding pocket in one of the 50 docking experiments performed using the wild type and mutant TRPV1 structures. *H–L*, fifty superimposed configurations generated by docking of PI(4,5)P$_2$ into the wild-type and R575A, R579A, K694A, and R701A mutants (*C*, *H*: Wild-type TRPV1, score 0; *D*,*I*: R575A, score 12.5; *E*, *J*: R579A, score 7.5; *F*, *K*: K694A, score 11.5; *G*, *L*: R701A, score 2.3). The TRPV1 wild-type and alanine TRPV1 mutants are shown in a *white cartoon representation*, while PI(4,5)P$_2$ is represented by a *stick model* in which carbon, oxygen, and phosphorus atoms are shown in *cyan*, *red*, and *brown*, respectively. A similar representation is used for amino acids of interest, except that the carbon atoms are shown in *yellow*.

The HOLE algorithm was used to determine whether changes in the internal radius of the TRPV1 channel pore caused by PI(4,5)P$_2$ binding, could be observed during in MD simulation. Beginning with the experimentally determined APO-TRPV1 structure embedded in a membrane, we added PI(4,5)P$_2$, and performed 300 ns of MD simulation. Then CAP was added to the system and the MD was extended 200 ns to stabilize the complex APO-TRPV1-PI(4,5)P$_2$-CAP. As shown in Fig. 4*C*, the results showed that the pore diameter in the area named lower-gate by Cao *et al.* (9) gradually increased at the end of 530 ns of simulation, after apply a restrain on Ile-679 to accelerate the gating process (Fig. 4*C*). The diameter of the lower-gate obtained has a greater values than those observed for the experimentally determined CAP-TRPV1 open structure. This increased radius allows us to argue that PI(4,5)P$_2$ directly leads to increased channel conductance, attributable to the displacement of the S6 transmembrane that "breaks" the hydrophobic seal formed by residues Thr-685 to Ile-696 (Fig. 4*C*).

To understand how the charge distribution of the amino acids surrounding the binding site may modulate interactions between PI(4,5)P$_2$ and the wild-type TRPV1 channel, the three-dimensional electrostatic potential of the equilibrated complex was calculated and averaged over the trajectory. The resulting electrostatic potential was projected over the surface of the APO-TRPV1 channel (Fig. 4*D*). The residues surrounding the PI(4,5)P$_2$ binding pocket created an overall positive potential in their vicinity. The residues that predominantly contributed to the electrostatic potential of the binding site were Gln-561, Lys-571, Arg-575, Arg-579, Lys-688, and Lys-694. Additionally, it was possible identify a hydrophobic area near the PI(4,5)P$_2$ hydrocarbon chains, which may have also contributed to the stabilization of the TRPV1-PI(4,5)P$_2$ complex.

Fig. 4*E* shows the PI(4,5)P$_2$ position proposed here (red) and the position for CAP (cyan) proposed by Cao *et al.* (9). These two models suggest that simultaneous binding of PI(4,5)P$_2$ and CAP is possible, with the two compounds separated by 4.3 Å at their closest contact. Fig. 4, *F* and *G* show a comparison between the PI(4,5)P$_2$ docking calculations into the APO-TRPV1 and CAP-TRPV1 experimental structure, respectively. These conformations showed that the CAP-TRPV1 experimental structure (Fig. 4*F*) favored PI(4,5)P$_2$ binding more than

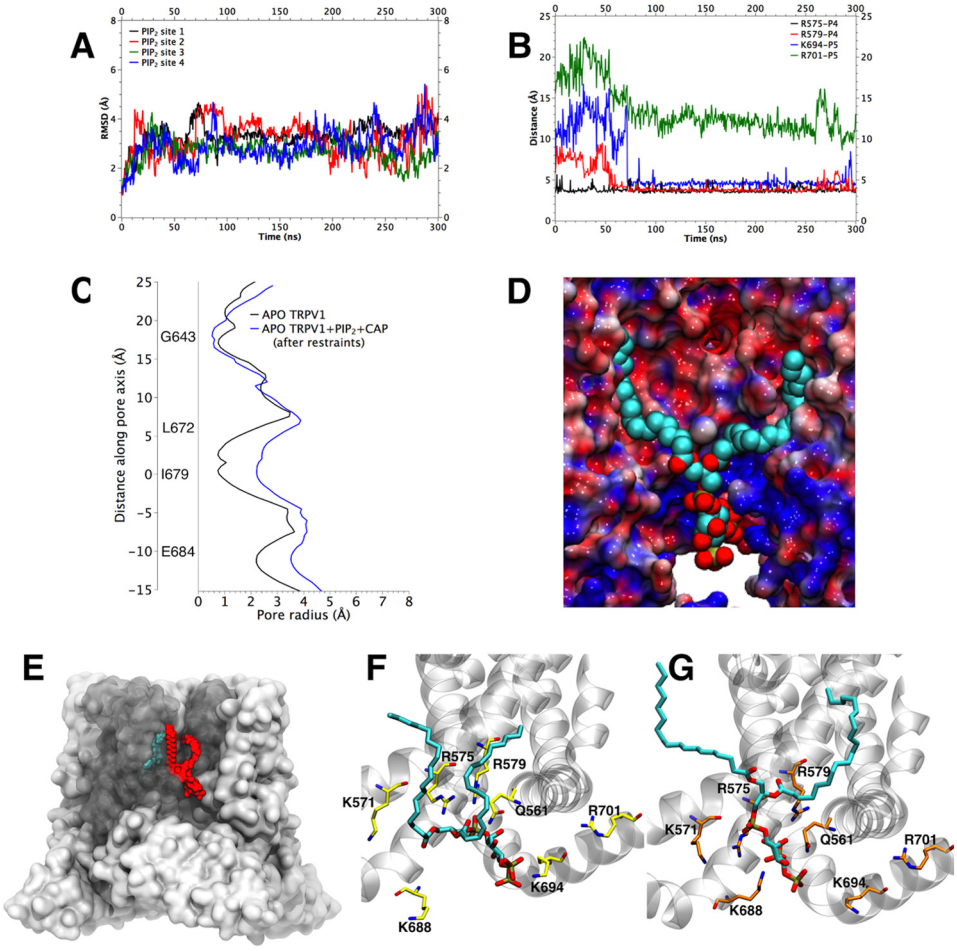

FIGURE 4. **Stability of PI(4,5)P_2 in its binding site, electrostatic potentials and the effect of PI(4,5)P_2 and CAP binding on the conformation of TRPV1.** *A*, root-mean-square deviation of the atomic coordinates of each of the PI(4,5)P_2 molecules during and MD simulation with respect to the positions identified by docking. *B*, distances between key residues of TRPV1 (Arg-575, Arg-579, Lys-694, and Arg-701) and each of the PI(4,5)P_2 phosphate groups as function of time Phosphate groups are identified as in Fig. 2*C*. *C*, pore radius along TRPV1's channel axis for different experimental structures: RTX-TRPV1 (*blue*), CAP-TRPV1 (*green*), and APO-TRPV1 (*red*). *C*, radius of APO-TRPV1 (PDB:3J5P) pore in the absence of ligands (*black line*) and in the presence of CAP and PI(4,5)P_2 (*blue line*). The *black line* was obtained from the last frame of the simulation of the complex APO-TRPV1+ PI(4,5)P_2+CAP using distances restraints. *D*, projection of the calculated electrostatic potential onto the surface of the TRPV1 channel. *E*, spatial location of the putative binding site for PI(4,5)P_2 (*red*) and CAP (*cyan*). Position of PI(4,5)P_2 determined by docking into the APO-TRPV1 (*F*) and CAP-TRPV1 experimentally determined structures (*G*).

the APO-TRPV1 experimental structure (Fig. 4*G*). In the former case, the entrance of PI(4,5)P_2 into the binding pocket was facilitated. The CAP-TRPV1 structure improved PI(4,5)P_2 affinity energy by an ICM score of −2.7, presenting a distance of 4 Å between the phosphate at position 5 of the PI(4,5)P_2 headgroup and residue Lys-694, as well as a distance of 6 Å in relation to residues Arg-575, Arg-579, and Gln-561, while a distance of 8 Å was found with respect to the Lys-688 residue. These results indicate that PI(4,5)P_2 binds with greater affinity to the TRPV1 channel after the channel binds CAP.

The results obtained by docking simulations were used as a starting point for MD simulations. The TRPV1-PI(4,5)P_2 configuration obtained by docking represents a hypothetical interaction before the conformational perturbation generated by PI(4,5)P_2 because the protein was kept fixed during docking. In MD simulations, we observed a fast decrease in TRPV1-PI(4,5)P_2 pair interaction energy (data not shown), due to relaxation of PI(4,5)P_2 and the residues Arg-575, Arg-579, and Lys-694. Lys-694 was the amino acid found to be altered the most from its initial conformation, which could be related to the bending mechanism of the segment S6-TRP domain (see Discussion). The strong interaction between phosphates of PI(4,5)P_2 and residues Arg-575, Arg-579, and Lys-694 is observed over 60% of time in APOTRPV1: PI(4,5)P_2 (Fig. 5*A*) and RTX/DkTx:TRPV1:PI(4,5)P_2 (Fig. 5*B*) simulations. The interaction between the residues Arg-575, Arg-579, and Lys-694 and PI(4,5)P_2 is clearly seen, even if the initial conformation of TRPV1 in molecular dynamics simulation starts from "closed state" (APO TRPV1) (Fig. 5*A*) or "open state" (RTX-DkTx TRPV1) (Fig. 5*B*). The distances between PI(4,5)P_2 and Arg-575, Arg-579, and Lys-694 residues located in the different subunits are less than 3 Å during most of the molecular dynamics simulation time (Fig. 5, *A* and *B*). Arg-575 shows the largest interaction time in both molecular dynamics simulations, reaching the 100% of time in contact with PI(4,5)P_2. In agreement with the electrophysiological results (Fig. 3), the residue R701 there in no interaction with PI(4,5)P_2 along the simulation. On the other hand, the absence (Fig. 5*A*) and presence (Fig. 5*B*) of Capsaicin does not affect the high percentage of

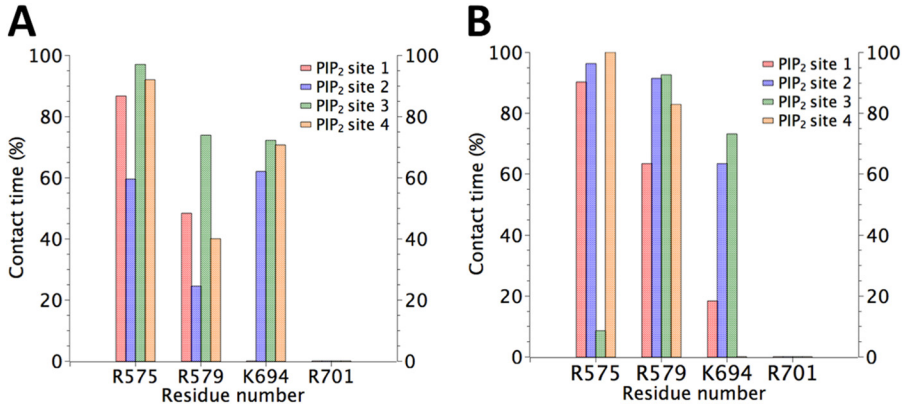

FIGURE 5. **Statistical analysis of the residues in contact with the phosphates groups of PI(4,5)P_2.** The contact time is represented as the percentage of the time of the full molecular dynamics simulation in which the amino acid residue indicated in the abscissa interacts with the phosphate groups of PI(4,5)P_2. A distance between the amino acid residue and PI(4,5)P_2 less than 3 Å is considered as a contact. Four PI(4,5)P_2 molecules were located in the four identical binding pockets designed Site 1, 2, 3, and 4. *Panel A* shows the data from simulation APO-TRPV1+ PI(4,5)P_2 and *B* is the result from RTX-DkTx TRPV1 PI(4,5)P_2+CAP trajectory. The negatively charged headgroup of PI(4,5)P_2 shows a high frequency of interaction with the residues Arg-575, Arg-579, and Lys-694. Residue Arg-701 has negligible contact with PI(4,5)P_2.

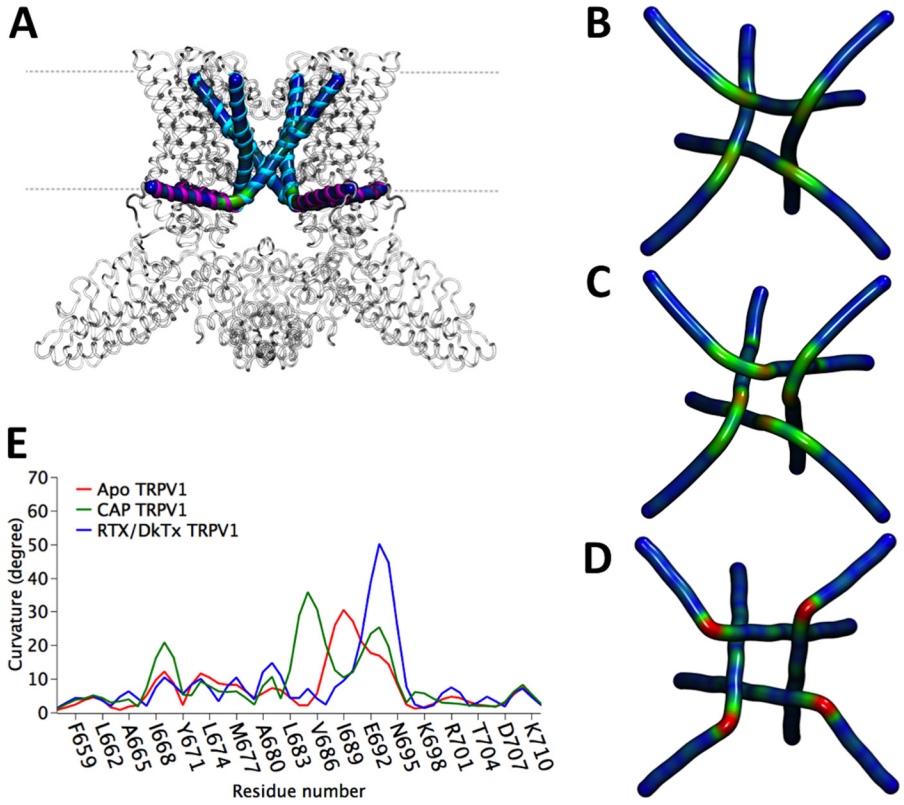

FIGURE 6. **Internal gate curvature of cryo-EM structures** *A*, curvature analysis of residues 656 to 712, in the S6-TRP domain, where the S6 segment is shown in *purple* and the TRP domain in *cyan*, as defined by Liao *et al.* (10). *B*, *bottom view* of the S6-TRP domain helix of the APO-TRPV1 structure (PDBid: 3J5P), (*C*) CAP-TRPV1 (PDBid: 3J5R) and (*D*) RTX-DkTx TRPV1 structures (PDBid: 3J5Q). Curvatures over 30° are highlighted in *green* and over 50° are shown in *red*. *E*, measurements of the bending angle in the S6-TRP domain of the cryo-microscopy structures were calculated using the VMD Bendix package (48).

interaction of phosphates groups of PI(4,5)P_2 and Arg-575, Arg-579, and Lys-694 amino acids.

DISCUSSION

How Does PI(4,5)P_2 Regulate TRP Channels?—Most TRP channels are modulated by PI(4,5)P_2 (30, 31). However the detailed molecular mechanisms by means of which this lipid regulates channel activity are still unknown. All we can say a priori with a relatively high degree of certainty is that electrostatics plays a fundamental role in PI(4,5)P_2 binding to proteins and all that is needed, in principle, is a cluster of basic residues that can serve as a site of attraction for multivalent negatively charged phosphoinositides (32, 33). In fact, basic residues in the TRP domain in the TRPM8 proximal region of the C terminus, as well as TRPV5 and TRPM5 are involved in protein-lipid interaction (34). PI(4,5)P_2 also activates TRPM4 (35, 36). In the latter case, however, the basic residues involved in the interaction with PI(4,5)P_2 were suggested to reside in a pleckstrin

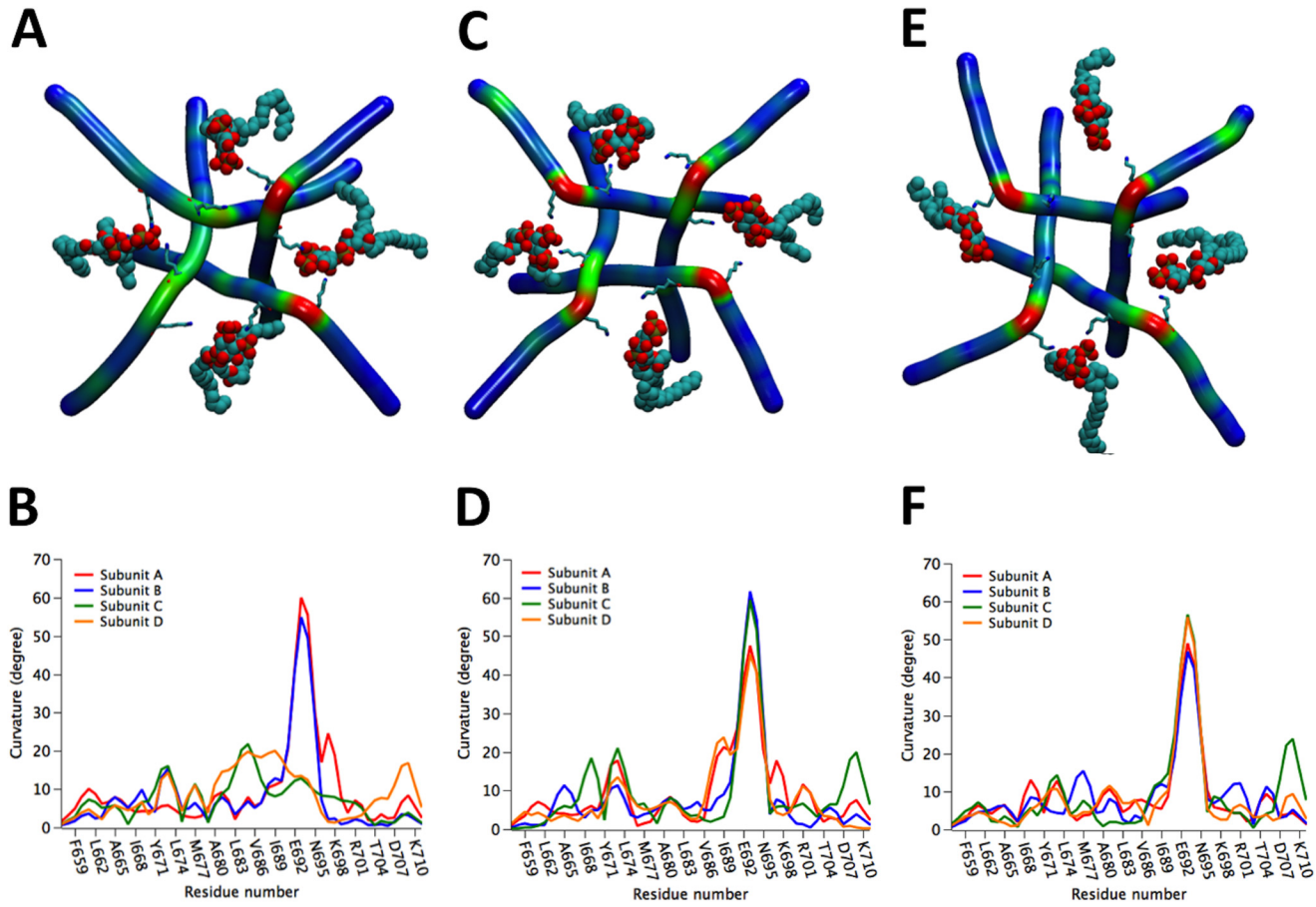

FIGURE 7. **Bending angle analysis of the fragment S6-TRP domain (residue 656 to 712) after molecular dynamics simulations.** *A*, simplified bottom view of the four subunits of the experimental APO-TRPV1structure after the addition of PI(4,5)P_2 and 300 ns of subsequent molecular dynamics simulation in a phospholipid membrane. *B*, bending angles shown for each residue of the segment S6-TRP domain. Two of the four subunits reached the bending angle expected for the open state of TRPV1 (about 50°). *C* and *D* show the experimental APO-TRPV1structure after the addition of PI(4,5)P_2 and CAP and a subsequent molecular dynamics simulation of 200 ns. At the end of this simulation, the four subunits reached the bending angle for the TRPV1open state. Finally, *E* and *D* show the final conformation obtained for the experimental RTX-DkTx TRPV1 structure after the addition of PI(4,5)P_2 and CAP and 40 ns of subsequent molecular dynamics simulation. They reached a steady conformation after just 5 ns and maintained the open conformations during the entirety of the simulation.

homology domain (*i.e.* [KR]-X(3–11)- [KR]-X-[KR]- [KR]) located toward the distal end of the C terminus (35). PI(4,5)P_2 also potentiates TRPV4 responses to heat and hypotonic stimuli. However, the neutralization of basic residues located in a sequence, resembling a phosphoinositide-binding site in the N terminus, is that which renders the channel unresponsive to hypotonicity and heat (37).

The TRPV1- PI(4,5)P_2 Conundrum—PI(4,5)P_2 was initially proposed to have a TRPV1 inhibitory role and a putative PI(4,5)P_2 binding site in the TRPV1 distal part of the C terminus was identified (38, 39). However, several reports have questioned the inhibitory effect of PI(4,5)P_2 on TRPV1. First of all, lack of recovery from desensitization due to the inhibition of phosphatidylinositol-4-kinase was observed. More importantly, truncation of the distal C-terminal region containing the alleged PI(4,5)P_2 binding site does not affect recovery from desensitization as compared with the wild-type (40). Second, the direct application of PI(4,5)P_2 to the internal side of a patch expressing TRPV1 channels has been reported to lead to channel activation, and the sequestration of PI(4,5)P_2 with polysine has been seen to inhibit channel activation (14, 41, 42). Finally, Ufret-Vincenty *et al.* (13) showed that PI(4,5)P_2 is able to directly activate TRPV1 channels, even after the removal of the distal C terminus, which suggests that the proximal C terminus would be involved in PI(4,5)P_2 binding.

Although the experiments performed in excised patches strongly support the role of PI(4,5)P_2 as a TRPV1 channel activator, the debate still continues. Lukacs *et al.* (42) showed that PI(4,5)P_2 may behave as an activator at high CAP concentrations, but as an inhibitor at low concentrations of the agonist. More recently, Cao *et al.* (15) were able to reconstitute the TRPV1 channel into liposomes and showed that if the liposomes were formed by a lipid mixture containing 4% PI(4,5)P_2, TRPV1 activity would be inhibited compared with liposomes lacking the phosphoinositide. These reconstitution experiments have been questioned on the basis of a promiscuous activation of TRPV1 by negatively charged lipids (12) and an inhibitory effect of PI(4,5)P_2 when present at high concentrations in the external lipid bilayer leaflet (43). It was further found that when TRPV1 was reconstituted into bilayers containing only neutral lipids, channel activation mediated by capsaicin depended on the presence of PI(4,5)P_2 (12).

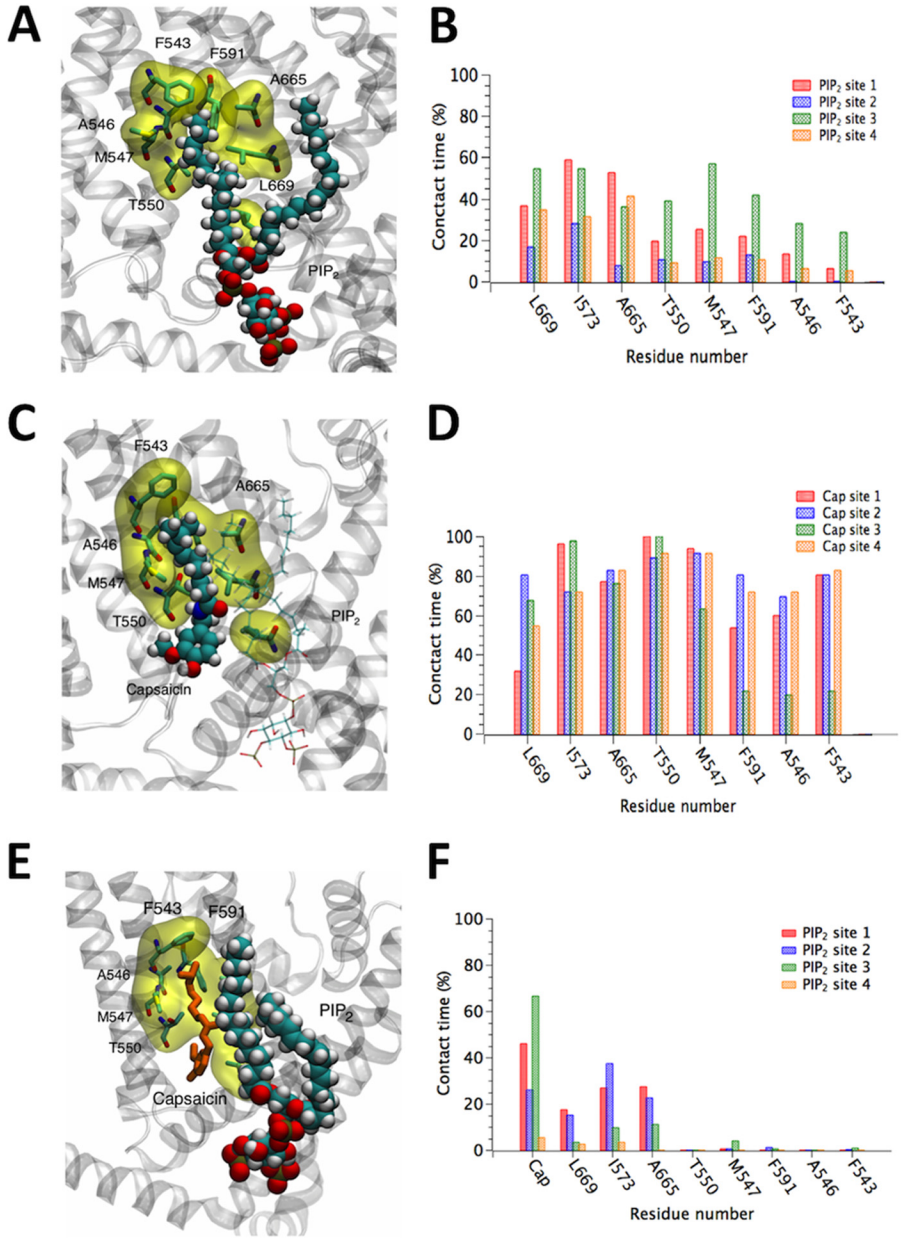

FIGURE 8. **Bound PI(4,5)P_2 can partially occlude the nearby CAP binding site.** *A*, snapshot from an MD simulation in which PI(4,5)P_2 is bound to the binding site determined in the present work. Here, in the absence of CAP, an aliphatic chain of PI(4,5)P_2 occupies the hypothesized CAP binding site. Atoms of PI(4,5)P_2 are shown as *spheres*, while residues of TRPV1 that may be in contact with both bound PI(4,5)P_2 and bound CAP are shown by a *stick model* and highlighted by a *yellow surface*. *B*, percentage of time in which atoms of PI(4,5)P_2 make contact with specific residues of the CAP binding site in the absence of CAP. Occupancy of the CAP binding site by the aliphatic chain of PI(4,5)P_2 is only partial, and it frequently exits and reenters this site. This suggests that bound PI(4,5)P_2 may partially, but not completely, block the access of CAP to its binding site. *C*, snapshot from an MD simulation where both CAP and PI(4,5)P_2 occupy their respective binding sites. Atoms of CAP are shown as *spheres*, while PI(4,5)P_2 is represented by *thin lines*. *D*, percentage of time in which atoms of CAP make contact with specific residues of its binding site while PI(4,5)P_2 is bound nearby. CAP stably occupies the hypothesized binding site. *E*, another snapshot from the same simulation represented in *panel C*, highlighting contact between PI(4,5)P_2 and CAP. Atoms of PI(4,5)P_2 are shown as *spheres*, while CAP is represented by *thin orange tubes*. *F*, percentage of time in which atoms of PI(4,5)P_2 make contact with specific residues of the CAP binding site while occupied by CAP. The presence of CAP substantially reduces the occupation of the site by the PI(4,5)P_2 aliphatic chain, which can be clearly seen by comparing to *panel B*.

Inferences about the Structural Basis of PI(4,5)P_2 Activation in the TRPV1 Channel—Binding to the C terminus is particularly interesting, due to its vicinity to the internal gate, as proposed by Cao *et al.* (9). However, the structural nature of the PI(4,5)P_2 binding site(s) and the mechanisms involved in the modulation of TRP channel gating mediated by the lipid are at present unknown. It is important to note here that MacKinnon's group (44) reported the crystal structure of the inward rectifier, Kir2.2, in complex with a PI(4,5)P_2 analog. In this case, PI(4,5)P_2 binds at the interface between the transmembrane domain and the cytoplasmic domain and a comparison between the Kir2.2 (APO) crystal structure and the bound PI(4,5)P_2 shows that phosphoinositide binding promotes a large (6 Å) displacement of the cytoplasmic domain, becoming joined to the transmembrane domain. We have compared the PI(4,5)P_2 binding site described here to the crystallographic structure of the Kir2.2 channel in complex with PI(4,5)P_2 molecules. Although the Kir2.2 channel is structurally distinct from

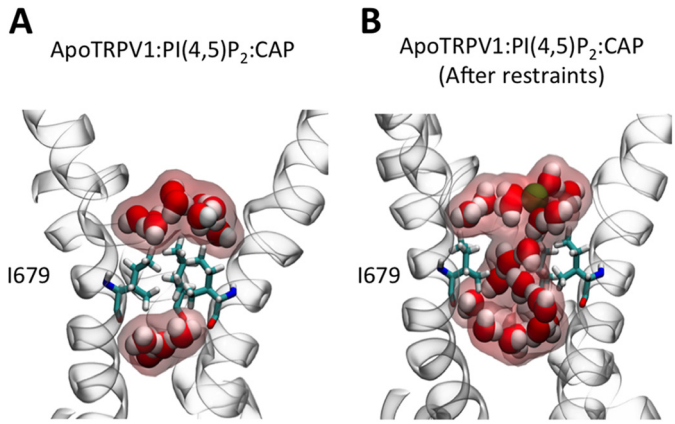

FIGURE 9. **CAP and PI(4,5)P_2 expand theTRPV1 pore radius at the internal gate level.** *A*, structure of the hydrophobic seal formed by I679 observed in the MD of the complex APO-TRPV1+ PI(4,5)P_2+CAP after 200 ns of MD simulation (before gate opening). *C*, at 40 ns of MD simulation after the addition of PI(4,5)P_2 and CAP the hydrophobic seal brakes (the pore increases in radius) allowing water to permeate.

TRPV1, it is similar to TRPV1 in that its crystallographic structure exhibits four PI(4,5)P_2 binding sites located at the interface between the transmembrane domain (TMD) and the cytoplasmic domain (CTD), lined with positive residues (mainly Arg and Lys) in each of the four subunits (44). Both structures (*i.e.* TRPV1-PI(4,5)P_2 and Kir2.2-PI(4,5)P_2) have been superimposed with respect to the ionic pore. We found that both binding sites are lined with basic residues and are located in the headgroup region of the intracellular bilayer leaflet. Indeed, the PI(4,5)P_2 headgroup's center of mass along the pore axis in the Kir2.2 experimental structure (44) differed by only 0.52 Å from the structure produced by docking PI(4,5)P_2 into TRPV1.

In the TRPV1-binding pocket, phosphate groups of PI(4,5)P_2 make contact with basic residues Arg-579 and Arg-575 from one subunit and Lys-694 from an adjacent subunit (Fig. 2*D*). Contrary to previous results, we show here that only Lys-694 in the TRP domain is part of the PI(4,5)P_2 binding site and that Arg-701 plays no role in binding, but it may help in stabilizing the binding pocket once it is formed. It is interesting to note here that in KCNQ (Kv7.2) channels, as in TRPV1, PIP_2 interacts with positive charges contained in the S4-S5 linker only when channel are open but with the S2-S3 linker in the closed state (45). In Kv channel the S4-S5 linker interacting with S6 (46) plays an important role in channel gating (47).

Fig. 6 shows the main difference between the internal TRPV1 gate (9, 10) in the closed and open configurations, namely the appearance (in the open configuration) of a pronounced bending of the α-helical constituting the S6 transmembrane domain and the TRP domain (Fig. 6*A*). This structure presents a 30.5° curvature at the level of residues Thr-685 to Ile-696 (max. bending at I689) when the internal gate is closed (APO, PDB: 3J5P; Fig. 6, *B* and *E*). The bending increases to 50.1° at the level of residues Asn-687 to Trp-697 (max. bending S693) when the upper and lower gates are open (RTX/DkTx, PDB: 3J5Q, Fig. 6, *D* and *E*). In the intermediate state of gating, and only when the lower gate is open (CAP, PDB: 3J5R), two maximum bending degrees in angles in residues Thr-685 (35.8°) and Ser-693 (25.3°) were observed (48) (Fig. 6, *C* and *E*). We performed a 300-ns molecular dynamics simulation, starting with the closed state of APO-TRPV1 in the presence of PI(4,5)P_2. We found that after 140 ns of simulation, two of the α-helical attained curvatures very similar to what we found in the open state of RTX-TRPV1 (cf., Fig. 6*D* and Fig. 7, *A* and *B*). Interestingly, when CAP was added to this simulation, we found three bent chains after only 66 ns, after which the structure remained stable for the remaining 200 ns of molecular dynamic simulation (Fig. 7, *C* and *D*). At 133 ns of this simulation (APO-TRPV1+PI(4,5)P_2 +CAP), the four subunits reached curvatures higher than 45° degrees, two of which approached 60° (S693) and the other two were close to 45° and showed a shoulder greater than 21° (Ile-689) (Fig. 6*D*). To compare this conformation with the experimental structure of the TRPV1 open state, we performed a simulation by using the TRPV1 structure with the upper and lower gate open (RTX/DkTx) in the presence of PI(4,5)P_2 and CAP, both fitted to this structure by means of docking simulations. After 40 ns of simulation, the curvature of the four chains reached over 50° (Fig. 7, *E* and *F*), similar to the conformation reached by the APO-TRPV1+PI(4,5)P_2+CAP) system.

Our experiments show differences in TRPV1 activation depending on whether PI(4,5)P_2 is added before or after CAP (Fig. 1*E*). We found that the current induced by PI(4,5)P_2 when CAP was added after PI(4,5)P_2 was always smaller than the TRPV1-induced currents when CAP was added prior to PI(4,5)P_2. In that context, when simulating the PI(4,5)P_2 complexed to the experimentally determined APO-TRPV1 structure, we observed that one of the PI(4,5)P_2 aliphatic chains strongly interacted with the CAP-binding pocket (Fig. 8, *A*–*D*). The presence of bound PI(4,5)P_2 may therefore partially obstruct the CAP-binding pocket, slowing the kinetics of CAP binding and possibly explaining the difference in TRPV1 activation when PI(4,5)P_2 is added before or after CAP.

The TRPV1 structure shows that residue Ile-679 forms a hydrophobic seal (lower gate) that expands in the presence of the agonist resineferatoxin and the scorpion toxin double-knot (DkTx) to a diameter of 9.3 Å (9, 10). Our MD simulations showed that the interaction between PI(4,5)P_2 and basic residues beneath the gate promotes the necessary structural changes to open it. The increase in curvature at the junction between the S6 and the TRP domain (the helical "elbow") (9) promotes a displacement of S6 that "breaks" the hydrophobic seal formed by Ile-679 (Fig. 4, *A*–*C*). To understand the intermediate states that lead to the expansion of the lower gate, we performed an extension of our molecular dynamics simulation (30 ns) using soft restraints that move the Cα carbon atom of Ile-679 from the close to the open conformation. During this process we observed that the radius of the pore increase from 0.8 Å (APO, blue line) to 2.2 Å (black line, APO-TRPV1 +PIP_2 +CAP) (Fig. 4*C*). During the first 10 ns the side chains of Ile-679 remain in contact. However, at the end of this period the Ile-679 side chains begin to collapse over the surface of the pore allowing the passage of water molecules through the hydrophobic seal (cf. Fig. 9, *A* and *B*).

REFERENCES

1. Caterina, M. J., Schumacher, M. A., Tominaga, M., Rosen, T. A., Levine, J. D., and Julius, D. (1997) The capsaicin receptor: a heat-activated ion channel in the pain pathway. *Nature* **389,** 816–824
2. Hayes, P., Meadows, H. J., Gunthorpe, M. J., Harries, M. H., Duckworth,

D. M., Cairns, W., Harrison, D. C., Clarke, C. E., Ellington, K., Prinjha, R. K., Barton, A. J., Medhurst, A. D., Smith, G. D., Topp, S., Murdock, P., Sanger, G. J., Terrett, J., Jenkins, O., Benham, C. D., Randall, A. D., Gloger, I. S., and Davis, J. B. (2000) Cloning and functional expression of a human orthologue of rat vanilloid receptor-1. *Pain* **88,** 205–215

3. Caterina, M. J., Leffler, A., Malmberg, A. B., Martin, W. J., Trafton, J., Petersen-Zeitz, K. R., Koltzenburg, M., Basbaum, A. I., and Julius, D. (2000) Impaired nociception and pain sensation in mice lacking the capsaicin receptor. *Science* **288,** 306–313
4. Davis, J. B., Gray, J., Gunthorpe, M. J., Hatcher, J. P., Davey, P. T., Overend, P., Harries, M. H., Latcham, J., Clapham, C., Atkinson, K., Hughes, S. A., Rance, K., Grau, E., Harper, A. J., Pugh, P. L., Rogers, D. C., Bingham, S., Randall, A., and Sheardown, S. A. (2000) Vanilloid receptor-1 is essential for inflammatory thermal hyperalgesia. *Nature* **405,** 183–187
5. Moriyama, T., Iida, T., Kobayashi, K., Higashi, T., Fukuoka, T., Tsumura, H., Leon, C., Suzuki, N., Inoue, K., Gachet, C., Noguchi, K., and Tominaga, M. (2003) Possible involvement of P2Y2 metabotropic receptors in ATP-induced transient receptor potential vanilloid receptor 1-mediated thermal hypersensitivity. *J. Neurosci.* **23,** 6058–6062
6. Baez-Nieto, D., Castillo, J. P., Dragicevic, C., Alvarez, O., and Latorre, R. (2011) Thermo-TRP channels: biophysics of polymodal receptors. *Adv. Exp. Med. Biol.* **704,** 469–490
7. Gaudet, R. (2008) TRP channels entering the structural era. *J. Physiol.* **586,** 3565–3575
8. Bohlen, C. J., Priel, A., Zhou, S., King, D., Siemens, J., and Julius, D. (2010) A bivalent tarantula toxin activates the capsaicin receptor, TRPV1, by targeting the outer pore domain. *Cell* **141,** 834–845
9. Cao, E., Liao, M., Cheng, Y., and Julius, D. (2013) TRPV1 structures in distinct conformations reveal activation mechanisms. *Nature* **504,** 113–118
10. Liao, M., Cao, E., Julius, D., and Cheng, Y. (2013) Structure of the TRPV1 ion channel determined by electron cryo-microscopy. *Nature* **504,** 107–112
11. Brauchi, S., Orta, G., Mascayano, C., Salazar, M., Raddatz, N., Urbina, H., Rosenmann, E., Gonzalez-Nilo, F., and Latorre, R. (2007) Dissection of the components for PIP2 activation and thermosensation in TRP channels. *Proc. Natl. Acad. Sci. U.S.A.* **104,** 10246–10251
12. Lukacs, V., Rives, J.-M., Sun, X., Zakharian, E., and Rohacs, T. (2013) Promiscuous activation of transient receptor potential vanilloid 1 (TRPV1) channels by negatively charged intracellular lipids: the key role of endogenous phosphoinositides in maintaining channel activity. *J. Biol. Chem.* **288,** 35003–35013
13. Ufret-Vincenty, C. A., Klein, R. M., Hua, L., Angueyra, J., and Gordon, S. E. (2011) Localization of the PIP2 sensor of TRPV1 ion channels. *J. Biol. Chem.* **286,** 9688–9698
14. Stein, A. T., Ufret-Vincenty, C. A., Hua, L., Santana, L. F., and Gordon, S. E. (2006) Phosphoinositide 3-kinase binds to TRPV1 and mediates NGF-stimulated TRPV1 trafficking to the plasma membrane. *J. Gen. Physiol.* **128,** 509–522
15. Cao, E., Cordero-Morales, J. F., Liu, B., Qin, F., and Julius, D. (2013) TRPV1 channels are intrinsically heat sensitive and negatively regulated by phosphoinositide lipids. *Neuron* **77,** 667–679
16. Simon, F., Leiva-Salcedo, E., Armisén, R., Riveros, A., Cerda, O., Varela, D., Eguiguren, A. L., Olivero, P., and Stutzin, A. (2010) Hydrogen peroxide removes TRPM4 current desensitization conferring increased vulnerability to necrotic cell death. *J. Biol. Chem.* **285,** 37150–37158
17. Humphrey, W., Dalke, A., and Schulten, K. (1996) VMD: visual molecular dynamics. *J. Mol. Graph.* **14,** 33–38, 27–8
18. Abagyan, R., Totrov, M., and Kuznetsov, D. (1994) ICM?A new method for protein modeling and design: Applications to docking and structure prediction from the distorted native conformation. *J. Comput. Chem.* **15,** 488–506
19. Abagyan, R., and Totrov, M. (1994) Biased probability Monte Carlo conformational searches and electrostatic calculations for peptides and proteins. *J. Mol. Biol.* **235,** 983–1002
20. Phillips, J. C., Braun, R., Wang, W., Gumbart, J., Tajkhorshid, E., Villa, E., Chipot, C., Skeel, R. D., Kalé, L., and Schulten, K. (2005) Scalable molecular dynamics with NAMD. *J. Comput. Chem.* **26,** 1781–1802
21. MacKerell, A. D., Bashford, D., Bellott, M., Dunbrack, R. L., Evanseck, J. D., Field, M. J., Fischer, S., Gao, J., Guo, H., Ha, S., Joseph-McCarthy, D., Kuchnir, L., Kuczera, K., Lau, F. T., Mattos, C., Michnick, S., Ngo, T., Nguyen, D. T., Prodhom, B., Reiher, W. E., Roux, B., Schlenkrich, M., Smith, J. C., Stote, R., Straub, J., Watanabe, M., Wiórkiewicz-Kuczera, J., Yin, D., and Karplus, M. (1998) All-atom empirical potential for molecular modeling and dynamics studies of proteins. *J. Phys. Chem. B* **102,** 3586–3616
22. Feller, S. E., Zhang, Y., Pastor, R. W., and Brooks, B. R. (1995) Constant pressure molecular dynamics simulation: The Langevin piston method. *J. Chem. Phys.* **103,** 4613
23. Essmann, U., Perera, L., Berkowitz, M. L., Darden, T., Lee, H., and Pedersen, L. G. (1995) A smooth particle mesh Ewald method. *J. Chem. Phys.* **103,** 8577
24. Vanommeslaeghe, K., Hatcher, E., Acharya, C., Kundu, S., Zhong, S., Shim, J., Darian, E., Guvench, O., Lopes, P., Vorobyov, I., and Mackerell, A. D. (2010) CHARMM general force field: A force field for drug-like molecules compatible with the CHARMM all-atom additive biological force fields. *J. Comput. Chem.* **31,** 671–690
25. Hénin, J., Shinoda, W., and Klein, M. L. (2008) United-atom acyl chains for CHARMM phospholipids. *J. Phys. Chem. B* **112,** 7008–7015
26. Klauda, J. B., Venable, R. M., Freites, J. A., O'Connor, J. W., Tobias, D. J., Mondragon-Ramirez, C., Vorobyov, I., MacKerell, A. D., Jr., and Pastor, R. W. (2010) Update of the CHARMM all-atom additive force field for lipids: validation on six lipid types. *J. Phys. Chem. B* **114,** 7830–7843
27. Jorgensen, W. L., Chandrasekhar, J., Madura, J. D., Impey, R. W., and Klein, M. L. (1983) Comparison of simple potential functions for simulating liquid water. *J. Chem. Phys.* **79,** 926
28. Brauchi, S., Orio, P., and Latorre, R. (2004) Clues to understanding cold sensation: thermodynamics and electrophysiological analysis of the cold receptor TRPM8. *Proc. Natl. Acad. Sci. U.S.A.* **101,** 15494–15499
29. Matta, J. A., and Ahern, G. P. (2007) Voltage is a partial activator of rat thermosensitive TRP channels. *J. Physiol.* **585,** 469–482
30. Gamper, N., and Rohacs, T. (2012) Phosphoinositide sensitivity of ion channels, a functional perspective. *Subcell. Biochem.* **59,** 289–333
31. Nilius, B., Owsianik, G., and Voets, T. (2008) Transient receptor potential channels meet phosphoinositides. *EMBO J.* **27,** 2809–2816
32. McLaughlin, S. (2006) Cell biology. Tools to tamper with phosphoinositides. *Science* **314,** 1402–1403
33. McLaughlin, S., and Murray, D. (2005) Plasma membrane phosphoinositide organization by protein electrostatics. *Nature* **438,** 605–611
34. Rohács, T., Lopes, C. M. B., Michailidis, I., and Logothetis, D. E. (2005) PI(4,5)P2 regulates the activation and desensitization of TRPM8 channels through the TRP domain. *Nat. Neurosci.* **8,** 626–634
35. Nilius, B., Mahieu, F., Prenen, J., Janssens, A., Owsianik, G., Vennekens, R., and Voets, T. (2006) The Ca2+-activated cation channel TRPM4 is regulated by phosphatidylinositol 4,5-biphosphate. *EMBO J.* **25,** 467–478
36. Zhang, Z., Okawa, H., Wang, Y., and Liman, E. R. (2005) Phosphatidylinositol 4,5-bisphosphate rescues TRPM4 channels from desensitization. *J. Biol. Chem.* **280,** 39185–39192
37. Garcia-Elias, A., Mrkonjic, S., Pardo-Pastor, C., Inada, H., Hellmich, U. A., Rubio-Moscardó, F., Plata, C., Gaudet, R., Vicente, R., and Valverde, M. A. (2013) Phosphatidylinositol-4,5-biphosphate-dependent rearrangement of TRPV4 cytosolic tails enables channel activation by physiological stimuli. *Proc. Natl. Acad. Sci. U.S.A.* **110,** 9553–9558
38. Chuang, H. H., Prescott, E. D., Kong, H., Shields, S., Jordt, S. E., Basbaum, A. I., Chao, M. V., and Julius, D. (2001) Bradykinin and nerve growth factor release the capsaicin receptor from PtdIns(4,5)P2-mediated inhibition. *Nature* **411,** 957–962
39. Prescott, E. D., and Julius, D. (2003) A modular PIP2 binding site as a determinant of capsaicin receptor sensitivity. *Science* **300,** 1284–1288
40. Liu, B., Zhang, C., and Qin, F. (2005) Functional recovery from desensitization of vanilloid receptor TRPV1 requires resynthesis of phosphatidylinositol 4,5-bisphosphate. *J. Neurosci.* **25,** 4835–4843
41. Klein, R. M., Ufret-Vincenty, C. A., Hua, L., and Gordon, S. E. (2008) Determinants of molecular specificity in phosphoinositide regulation. Phosphatidylinositol (4,5)-bisphosphate (PI(4,5)P2) is the endogenous lipid regulating TRPV1. *J. Biol. Chem.* **283,** 26208–26216

42. Lukacs, V., Thyagarajan, B., Varnai, P., Balla, A., Balla, T., and Rohacs, T. (2007) Dual regulation of TRPV1 by phosphoinositides. *J. Neurosci.* **27,** 7070–7080
43. Senning, E. N., Collins, M. D., Stratiievska, A., Ufret-Vincenty, C. A., and Gordon, S. E. (2014) Regulation of TRPV1 ion channel by phosphoinositide (4,5)-bisphosphate: the role of membrane asymmetry. *J. Biol. Chem.* **289,** 10999–11006
44. Hansen, S. B., Tao, X., and MacKinnon, R. (2011) Structural basis of PIP2 activation of the classical inward rectifier K+ channel Kir2.2. *Nature* **477,** 495–498
45. Zaydman, M. A., and Cui, J. (2014) PIP2 regulation of KCNQ channels: biophysical and molecular mechanisms for lipid modulation of voltage-dependent gating. *Front. Physiol.* **5,** 195–205
46. Long, S. B., Campbell, E. B., and Mackinnon, R. (2005) Voltage sensor of Kv1.2: structural basis of electromechanical coupling. *Science* **309,** 903–908
47. Zhang, Q., Zhou, P., Chen, Z., Li, M., Jiang, H., Gao, Z., and Yang, H. (2013) Dynamic PIP2 interactions with voltage sensor elements contribute to KCNQ2 channel gating. *Proc. Natl. Acad. Sci. U.S.A.* **110,** 20093–20098
48. Dahl, A. C. E., Chavent, M., and Sansom, M. S. P. (2012) Bendix: intuitive helix geometry analysis and abstraction. *Bioinformatics* **28,** 2193–2194